AFM Study on the Electric-Field Effects on Supported Bilayer Lipid Membranes

Lars J. C. Jeuken
Institute of Membrane and Systems Biology, University of Leeds, Leeds, United Kingdom

ABSTRACT Electric-field induced changes in structure and conductivity of supported bilayer lipid membranes (SLM) have been studied at submicroscopic resolution using atomic force microscopy and electrochemical impedance spectroscopy. The SLMs are formed on gold surfaces modified with mixed self-assembled monolayers of a cholesterol-tether and 6-mercaptohexanol. At applied potentials of ≤ -0.25 V versus standard hydrogen electrode, the conductance of the SLM increases and membrane areas of <150 nm in size are found to elevate from the surface up to 15 nm in height. To estimate the electric field experienced by the lipid membrane, electrowetting has been used to determine the point of zero charge of a 6-mercaptohexanol-modified surface (0.19 ± 0.13 V versus standard hydrogen electrode). The effects of electric fields on the structure and conductance of supported membranes are discussed.

INTRODUCTION

The effects of electric fields on the conductivity of cell membranes have been investigated since the 1940s, while electroporation began to mature into a discipline since 1975 (1,2). Despite this long history electric-field effects are still intensely studied, driven by the wide range of applications of electroporation, which permeabilizes cell membranes by pore formation. Under the right conditions, the formation of pores is reversible and this is the basis for numerous applications in the transfer of small molecules into and out of cells and vesicles (3). Electroporation is routinely used in biotechnology and has more recently found applications in medicine as a method for efficient drug delivery and selective destruction of malicious (cancer) cells.

In the absence of strong electric fields (i.e., under normal circumstances), the cell membrane is an exceptional barrier to polar molecules and ions. The conductivity of cell membranes is usually in the sub-mS/cm^2 range while that of pure lipid bilayers is typically 10^{-8} S/cm^2. This conductivity increases rapidly when electric fields are applied of 0.15–1 V across the membrane. For electroporation purposes, the pulsed electric field has been more successful and therefore commonly used (1,2). Recent progress has been reported on shortening of the pulse time (with an increase in electric field strength) toward the nanosecond time domain and on the molecular and structural nature of the permeabilization process. The latter research area has greatly benefited from theoretical approaches (e.g., see Krassowska and Filev (4)) and molecular dynamics simulations (5–8). The shortening of the pulse times has also been beneficial to the simulations as this has brought the experimental time domain within reach of that of molecular dynamic simulations (9). The results of the simulations suggest that the electroporation takes place in two stages. First, water penetrates the lipid bilayer, apparently at local defect locations, to form a wirelike structure. Second, the wires grow in size into water-filled pores in which the lipids reorganize around the pore to position the headgroup toward the water column. However, not all studies agree with the order of these two steps as some studies suggest that lipid reorientation constitutes the first step (10). Either way, the pore sizes are in the order of nanometers. On top of these theoretical advances, some groups have been able to study macro pores in giant unilaminar vesicles using confocal fluorescence microscopy. These pores are in the micron range and usually short-lived, although the lifetime can be extended by clever use of detergents or nonnatural phospholipids (11,12).

Despite these advances, the experimental visualization of pores created by most electroporating procedures—submicroscopic and short lived—has not yet been possible. Here, the effects of DC electric fields on supported lipid membranes (SLM) are studied at submicroscopic resolution using tapping-mode atomic force microscopy (AFM). AFM has been used with great success to study lipid membranes and membrane proteins (13–17). AFM as a tool to study SLMs prepared by vesicle fusion was first reported by Mou et al. (18,19) and recently reviewed by Dufrêne and Lee (20), and Connell and Smith (21), and Richter et al. (22). Typically, SLMs for AFM studies are prepared on mica, but to apply homogeneous electric fields to a SLM, the solid support needs to be conducting. Here, SLMs (or tethered membranes) are formed by spontaneous vesicle fusion on template-stripped gold surfaces modified with a cholesterol tether (see Fig. 1). To support the AFM results, the membrane conductivity has also been monitored using electrochemical impedance spectroscopy (EIS).

Submitted September 28, 2007, and accepted for publication February 8, 2008.

Address reprint requests to Lars J. C. Jeuken, Tel.: 44-0-113-343-3829; E-mail: l.j.c.jeuken@leeds.ac.uk.

Editor: Petra Schwille.

0006-3495/08/06/4711/07 $2.00

doi: 10.1529/biophysj.107.122887

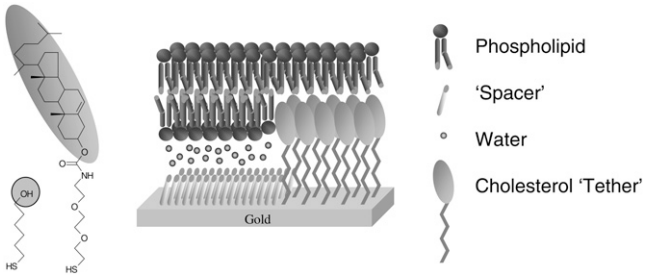

FIGURE 1 A schematic representation of the supported lipid membrane (SLM) used in this work. In this representation, the spacer and the cholesterol tether are shown to phase-separate on the surface, which was previously shown to occur on the 10–200 nm scale by friction AFM (25). Based on neutral reflectivity data from Valincius et al. (31) and McGillivray et al. (32) on a very similar SLM system, a thin layer of water has been included in the sublayer.

MATERIALS AND METHODS

Materials

EO3-cholestol was made as previously described (23). The chemicals 6-mercaptohexanol (6MH; Sigma, St. Louis, MO), 2-propanol, methanol (HPLC grade; Fisher Scientific, Pittsburgh, PA), and *E. coli* polar lipid extract were used as received. All electrochemical experiments were performed in 20 mM (3-(*n*-Morpholino)propanesulfonic acid buffer (Sigma) with 30 mM Na_2SO_4 adjusted to pH 7.4 with NaOH at 20°C. Vesicles were prepared by dispersing 5 g/L lipid in buffer, vortexing and extruding 11 times through 100 nm track-etched Nucleopore membranes (Avanti Polar Lipids, Alabaster, AL).

Template-stripped gold (TSG) surfaces were prepared according to Stamou et al. (24). In short, 150 nm of gold (Goodfellow, Oakdale, PA) was evaporated on a polished silicon wafer (Rockwood Wafer Reclaim, Riddings, Derbyshire, United Kingdom) using an Auto 306 evaporator (BOC Edwards, Wilmington, MA) at $<2 \times 10^{-6}$ mBar. The gold surfaces were then glued with EPO-TEK 377 to glass slides and cured for 120 min at 120°C. After cooling, the slides were detached from the silicon wafers to expose the TSG surface. Self-assembled monolayers (SAMs) were formed by directly immersing the substrate in 0.11 mM EO3-Cholesterol and 0.89 mM 6MH solution, in propanol, for 16 h. The samples were rinsed with propanol and methanol, dried under nitrogen, and used within several hours. It was shown previously that these surfaces contain ~60% EO3-Cholesterol and ~40% 6MH by area (25).

The quantity of 0.5 g/L vesicles in buffer were added to the modified gold surfaces in the presence of 10 mM $CaCl_2$ and left to incubate for 2 h. After bilayer formation, the surface was rinsed several times with buffer to remove remaining vesicles and 1 mM EDTA was added to one of the rinsing steps to remove Ca^{II} ions.

For the electrochemical contact angle measurement, the TSG samples were immersed in 1 mM 6MH, in propanol, for 16 h.

Instrumentation

Electrochemical impedance spectra (EIS) were obtained using a thermostated electrochemical cell of all-glass construction, with the main compartment housing the gold working electrode (imbedded in a PTFE holder with a rubber O-ring), a platinum wire counterelectrode, and a saturated calomel reference electrode (SCE, Radiometer, Copenhagen, Denmark). All potentials are quoted versus standard hydrogen electrode (SHE). The cell was enclosed in a Faraday cage to minimize electrical noise and purged with Argon to remove oxygen. EIS was recorded using an Autolab electrochemical analyzer (Eco-Chemie, Utrecht, The Netherlands) equipped with a PGSTAT30 potentiostat and a FRA2 frequency analyzer. The fits were preformed by a program that uses a Levenberg-Marquardt procedure and the errors in the parameters were analyzed using a Monte Carlo bootstrap method.

Tapping-mode AFM height images were recorded in an electrochemistry tapping mode fluid cell (Digital Instruments, Veeco Metrology Group, Santa Barbara, CA) at room temperature (23°C) using a Multimode AFM on a Nanoscope IIIa (Veeco) controller, equipped with a Universal Biopotentiostat (Veeco) and silicon nitride cantilevers (NP-S, Veeco Metrology Group). The electrochemical cell was fitted with a no-leak Ag/AgCl/3M KCl (ESA Analytical, Aylesbury, Bucks, United Kingdom) reference electrode and a platinum counterelectrode. The cantilevers had a spring constant of ~0.06 N/m. The height images reported here are raw, unfiltered data obtained by tapping (dynamic) mode at a frequency in the range 8–9 kHz. Force curves (z-Piezo extension versus cantilever deflection) were recorder under identical conditions and converted into true force-distance. Force curves were recorded before and after experiments to secure that a lipid membrane was indeed present (see Fig. 3 in (26) for an example).

The point of zero charge of TSG surfaces modified with 6MH was determined by measuring the contact angle as a function of applied potential using a method modified from that of Abbott et al. (27) and Iwami et al. (28). Advancing contact angles were obtained with a goniometer (First Ten Angstroms, Portsmouth, VA) and analyzed with FTA 4000 software (First Ten Angstroms). A drop was placed on the TSG gold surface via a thin needle and was constantly increased in volume while images of the drop were taken at exact time-intervals and analyzed afterwards. The drop volume remained always <0.5 μL. A no-leak Ag/AgCl/3M KCl (ESA Analytical) reference electrode and a platinum counterelectrode were inserted in the buffer by placing them in the liquid in front of the needle as schematically shown in Fig. 2. A four-electrode potentiostat (CHI604, CH Instruments, Austin, TX) was used to alter the applied potential at 100 mV/s, which was synchronized with images taken from the growing drop. We note that the potential of the no-leak reference electrode from ESA Analytical was calibrated and found to deviate several tens of mV from that expected for a Ag/AgCl/3M KCl reference electrode.

RESULTS

SLMs (or tethered membranes) were formed on template-stripped gold surfaces containing mixed self-assembled monolayers (SAMs) of EO3-cholestol and 6-mercaptohexanol (6MH) with a 60:40 distribution by surface area, respectively (see Fig. 1). The SLMs were prepared using a polar lipid extract from *E. coli*, which is negatively charged and rich in phosphatidyl-ethanolamine. Electric fields were generated by applying a DC potential versus a reference electrode using a standard four-electrode electrochemical setup, which was also used to measure the EIS data (all potentials are given versus a standard hydrogen electrode, or SHE).

Electrochemical impedance spectroscopy

Fig. 3 *A* shows the EIS results in the form of a Nyquist diagram and as a function of the applied direct-current potential. In the Nyquist diagram the semicircle diameter is equivalent to the transmembrane resistance of the SLM and can be seen to decrease when the applied potential decreases below ~0 V versus SHE.

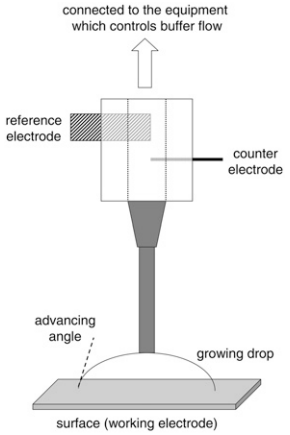

FIGURE 2 A schematic representation of the system used to measure the contact angle of an electrochemical surface at varying applied potentials. By placing the reference and counterelectrode into the electrolyte via the needle that is used to increase the drop volume to measure the advancing contact angle, the geometric influence of both electrodes is minimized.

Good fits of the EIS data are obtained using a $[R(Q_mR_mQ_d)C]$ equivalent circuit in which the elements in square brackets are in series and in round brackets in parallel and Q is a constant phase element (CPE), $Z = 1/Y_0(i\omega)^{\alpha}$. When analyzing the data with this equivalent circuit it was found that Q_d was characterized by a very low value of Y_0 and $\alpha \approx 0.5$ and was particularly required to accurately fit the low frequencies. This equivalent circuit is interpreted as follows: R is the solution resistance, Q_m is the double-layer capacitance of the SLM with a resistance of R_m. C is the capacitance of the surface without the membrane, and in almost all cases did not improve the fit significantly (although in some cases it did decrease the parameter R_m). Q_d is the double-layer capacitance of defects sites and, as the double-layer capacitance depends on the electrode area, the low value for Q_d reflects a low number of defects sites.

We have previously also modeled the EIS of SLM systems with a model that combines a CPE element with a Cole-Cole relaxation distribution (25),

$$Z_{C_{dl}} = \frac{1}{(i\omega)^{\beta}\omega_0^{1-\beta}\left[\dfrac{\Delta C}{1+(i\omega\tau)^{\alpha}} + C_{inf}\right]}, \quad (1)$$

in which C_{inf} is the double-layer capacitance of the SLM and ΔC the additional low frequency capacitance element with the relaxation time constant τ. The value ω is the impedance frequency, and α and β are variables that describe the symmetrical broadening of the relaxation and the frequency dispersion of the CPE element, respectively. The quantity $\omega_0 = 1\ s^{-1}$ is a dummy parameter to correct for units. When fitting the EIS data, it was found that the parameters ΔC and τ show a high degree of correlation. The parameter ΔC is therefore fixed to a value that gives the best fit for all spectra, and τ is fitted to reflect the change in relaxation properties of the SLM as a function of applied potential.

R_m and τ-values determined with both models are shown in Fig. 3 *B*, which shows that the faster relaxation (lower τ) at potentials <0.2 V is equivalent to an increase in conductivity of the SLM. When the potential is lowered to <–0.6 V versus SHE, the thiol-gold bond of the SAM is reduced and the SLM is destabilized. This results in a major drop in τ or R_m (note the break in the *y* axis of Fig. 3 *B*). However, the SLM is not immediately destroyed, since τ recovers when the potential is increased again (Fig. 3 *B*, *circles*). We note that a small irreversible change occurs when potentials <-0.2 V are applied. This change is characterized by a small increase in the double-layer capacitance of the SLM from ~0.8 to 1.0 μF/cm^2.

Atomic force microscopy

Tapping mode AFM of the SLM shows a featureless surface when potentials are gradually decreased from the open cell potential (usually ~0.2–0.3 V versus SHE) to −0.15 V, even though the EIS results indicate that at <0.2 V, the conductivity increases. A typical AFM height image is shown in Fig. 4 *A* and this image remains unaltered upon repeated scanning. However, when the applied potential is decreased to −0.25 V

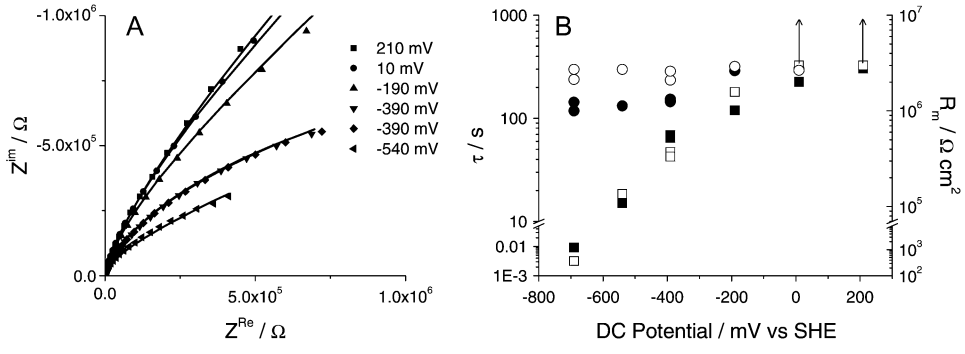

FIGURE 3 Electrochemical impedance spectroscopy (EIS) results of a SLM at varying DC potentials (surface area = 0.25 cm^2). (*A*) Nyquist plots of data from a SLM sample at DC potentials as indicated. The lines represent fits using Eq. 1. (*B*) Fit results of the EIS data. (*Squares*) Fit results of EIS data at varying DC potentials as shown in panel *A*. (*Circles*) Fit results of the EIS data measured after reversing the applied potential to 0.21 V. (*Open symbols*, *right axis*) R_m values using the equivalent circuit $R(Q_mR_mQ_d)C$, in which C has been fixed to 22 μF × cm^{-2} and α from Q_d to 0.5; and (*solid symbols*, *left axis*) τ-values using Eq. 1. Analysis using a Monte Carlo bootstrap method indicates the errors are smaller than the size of the data-points, except for the R_m values at 10 and 210 mV, for which only a lower limit can be given (indicated by the *arrows*).

or less, elevated areas of <150 nm in size appear, usually circular in shape and up to 15 nm in height (Fig. 4 *B*). These areas grow between subsequent scans, but, importantly, also disappear again. This is clearly visible in Fig. 5 in which individual heightened areas in subsequent scans (each taking 256 s) are shown. When the applied potential is returned to 0.05 V, the surface stabilizes but elevated areas are very slow to disappear, which could explain the small increase in the double-layer capacitance of the SLM.

To quantify the results, all peaks above ~3 nm were manually analyzed from one set of experiments consisting of 29 images at decreasing and increasing applied potentials. Forty-five locations were identified in a 1 μm^2 area in which heightened areas appeared. Note that the location of the heightened areas were fixed on the surface and did not migrate or fuse, thus allowing the individual tracking of these areas (see Fig. 5). Fig. 6 *A* (*square points*) shows the total number of heightened areas in a 1 μm^2 area as a function of applied potential and time. It is clear that the number of heightened areas is not only dependent on the applied potential, but also on how long this potential is applied. The number of peaks that appear or disappear is also shown (*circle* and *triangle data points*, respectively). This analysis indicates that the rate of appearance (and perhaps disappearance) is dependent on the applied potential. It would thus be possible that heightened areas might be formed even at potentials between 0.2 and −0.15 V, but with a rate too slow to be detected with AFM in a 1 μm^2 area.

The height and half-peak-width were determined for 403 heightened areas and Fig. 6 *B* shows their observed correlation. Note that small or very broad peaks might not have been detected and this is represented by the shaded area in Fig. 6 *B*. A sharp cutoff is visible in the ratio height/width and this defines the maximum sharpness at which peaks are observed. This maximum ratio is approximately indicated by the dashed line in Fig. 6 *B* and a height-width normalized profile of an area with maximum sharpness is shown in Fig. 6 *C*.

Electrochemical contact angle measurements

In the previous Results subsections, the field strength across the membrane was varied by changing the applied potential (versus SHE). However, the applied potential does not directly relate to the transmembrane potential across the membrane. To establish the transmembrane potential across the SLM, the applied potential needs to be offset against the interfacial point of zero charge (*pzc*) of the underlying solid substrate. For reasons that will become clear in the Discussion, the *pzc* of 6HM modified surfaces is of main interest. To measure the *pzc* of 6MH-modified gold surfaces, we followed a protocol similar to that published by Iwami et al. (28). Iwami and co-workers measured the static contact angle of a droplet of electrolyte while changing the applied potential on the surface. To change the applied potential, a small counter- and silver reference electrode were inserted into the droplet. This procedure was modified in that the advancing contact angle was determined and the reference and counterelectrodes were connected to the growing droplet as illustrated in Fig. 2. This simplified the procedure and minimized potential artifacts that might arise when electrodes are inserted directly in the droplet.

We note that for surfaces modified with 6MH, the variation in angle between drops (standard deviation is 3°) is almost as large as the variation induced by changing the applied potential. However, the trend with which the angle changes as a function of applied potential for each individual drop is reproducible. Fig. 7 shows the contact angles starting either from the lower or higher limit of the potential window (*solid* and *open points*, respectively). A clear hysteresis is observed that depends on the starting point of the experiment. The hysteresis seems to be due to a change of the SAM induced at potentials >0.4 V versus SHE, and is irreversible within the time domain of the experiment (12–14 s). After this change, the *pzc* cannot be accurately determined, and is <−0.4 V. In contrast, when the experiment is started at the low potential limit, a clear maximum in contact angle is observed at 0.19 V with SD 0.13 V. As the potential is never raised above 0.25 V in the EIS and AFM experiments, we assume that the *pzc* for 6HM-modified surfaces is ~0.2 V versus SHE.

DISCUSSION

It is important to note that AFM experiments were also conducted on SLMs that were formed on SAMs of only EO3-cholesterol. These SLM structures do not produce elevated areas, suggesting that the elevated areas are only formed on

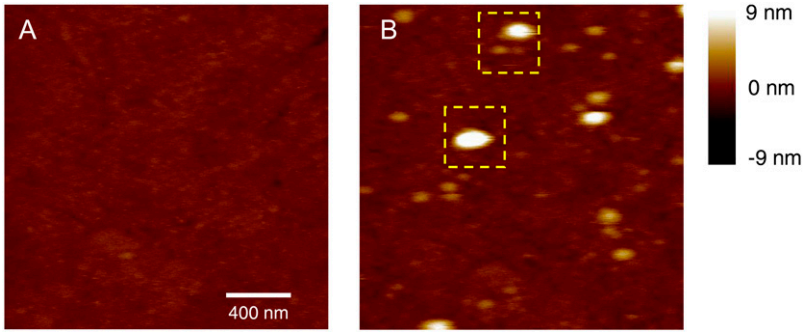

FIGURE 4 Electrochemical tapping mode AFM images (1 × 1 μm) of the same area of a SLM while applying either (*A*) −0.15 V or (*B*) −0.35 V versus SHE to the electrode surface. The images were recorded at 2 Hz under conditions described in Instrumentation. The dashed boxes refer to Fig. 5.

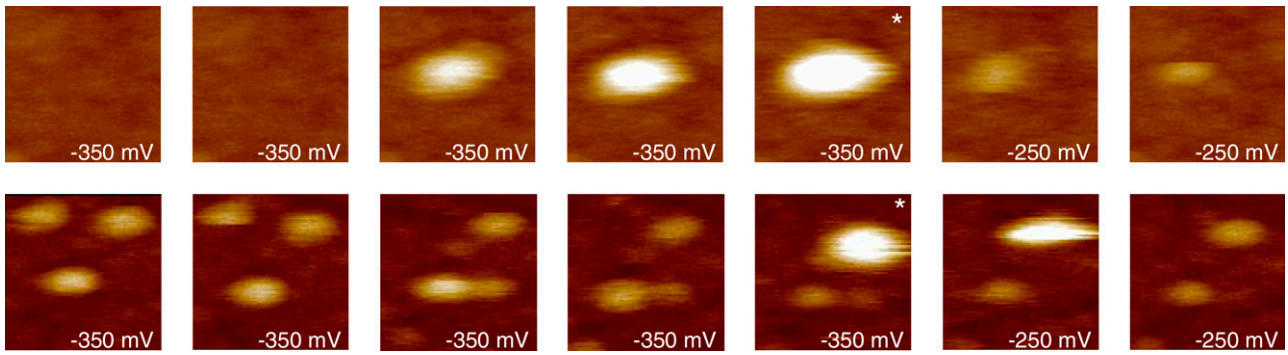

FIGURE 5 Two selected areas (indicated by *dashed boxes* in Fig. 4) of consecutive AFM images of a SLM at varying DC potentials. During each consecutive AFM image, the given potential was applied to the SLM. Each complete AFM images was taken of a 1×1 μm area at 2 Hz and took 256 s. Some additional time of $\sim$10 s was required between scans to optimize scan conditions. The size of the selected areas is $\sim 200 \times 200$ nm. The asterisk indicates the selected area taken from the same image as shown in Fig. 4 *B*.

parts of the surface which have been modified with 6MH (it was previously shown that SAMs of EO3-cholesterol and 6MH are phase-separated (25)). It is for this reason that the *pzc* was determined of 6MH-modified surfaces. To our knowledge, there is only one reported study on the electrowetting behavior of $-$OH terminated alkanethiols (29), in which the maximum contact angle or *pzc* was found at 0.7 V versus SHE, which is considerably higher than 0.2 V determined in this study. However, Sondag-Huethorst and Fokkink (29) used SAMs of 12-mercaptododecanol, which have a more crystalline character than 6MH. The relatively high advancing contact angle of 6MH (45–60° for buffer, compared to 25° for 12-mercaptododecanol; see Fig. 7) suggests that, due to chain disorder, the hydrophobic alkane chain of 6MH significantly contributes to the electrowetting properties of 6HM-modified surfaces. It has been shown that the *pzc* decreases with hydrophobicity (29), with the *pzc* of CH_3-terminated SAMs as low as -0.3 V versus SHE (28,29). We speculate that the less crystalline character of 6MH is also responsible for the observed hysteresis in Fig. 7, which might be due to oxidative damage of the thiol groups.

When the potential is applied equal to the *pzc*, a membrane adsorbed on top of the 6MH will not experience an electric field other than that created by the membrane itself. When a potential other than the *pzc* is applied to the SLM, the membrane will experience an electric field proportional to the difference between the applied potential and the *pzc*. The potential drop across the 6MH layer will decrease the electric field experienced by the lipid membrane. However, the potential drop across the thin 6MH layer is likely to be much smaller than across the much thicker lipid bilayer. Sondag-Huethorst and Fokkink (29) have described another issue that might decrease the electric field experienced by the lipid membrane. They found a discrepancy between the calculated surface tension of 12-mercaptododecanol SAMs using either electrowetting or surface capacitance values and speculated that the tilt angle of the SAM might change under the influence of the electric fields. They discarded the possibility that the discrepancy is due to ion penetration into the SAM, although Boubour and Lennox (30) later showed that this is also possible. Nonetheless, for the purpose of the work reported here, either explanation will result in a further reduction of the electric field experienced by the membrane at a given applied potential. Finally, as already noted in Results, the onset on heightened areas is observed at -0.25 V, but these areas might also be formed at a slower rate above -0.25 V versus SHE. In conclusion, it can be estimated that the onset of heightened areas as observed by AFM starts at an electric field of ≤ 0.45 V ($= |-0.25\ \text{V} - pzc|$) across the membrane.

The analysis of the heightened areas strongly suggests that they are limited in sharpness. A normalized height-length profile of an area with maximum sharpness is shown in Fig. 6 *C* and is still very shallow, as expected for a curved phospholipid membrane. The sharpness of a heightened area could be limited by the maximum curvature of the phospholipid membrane. The width of the heightened areas is most likely limited by the properties of the mixed SAM (EO3-Cholesterol and 6MH), which phase-separates on the 1–200-nm length scale, as previously measured with friction AFM (25).

When potentials at <0 V versus SHE are applied, ions are increasingly able to penetrate the membrane as shown by EIS. We note that an extensive EIS study has been performed of alkanethiol SAMs by Boubour and Lennox (30), who concluded that below a critical applied potential, a transformation occurs in the SAM that results in a decrease in resistance. They suggest that this is due to a structural change in the SAM that allows ions to penetrate the well-packed alkane chains. The exact nature of the structural change is unknown. Despite the large difference between a relatively simple SAM and the SLM system studied here, the EIS results are remarkably similar in nature.

Several hypotheses could explain the formation of heightened areas as a function of transmembrane potential. In the absence of an electric field, a SLM is formed with a limited amount of water in the sublayer (31,32), which is the layer between the phospholipid bilayer and the areas of the

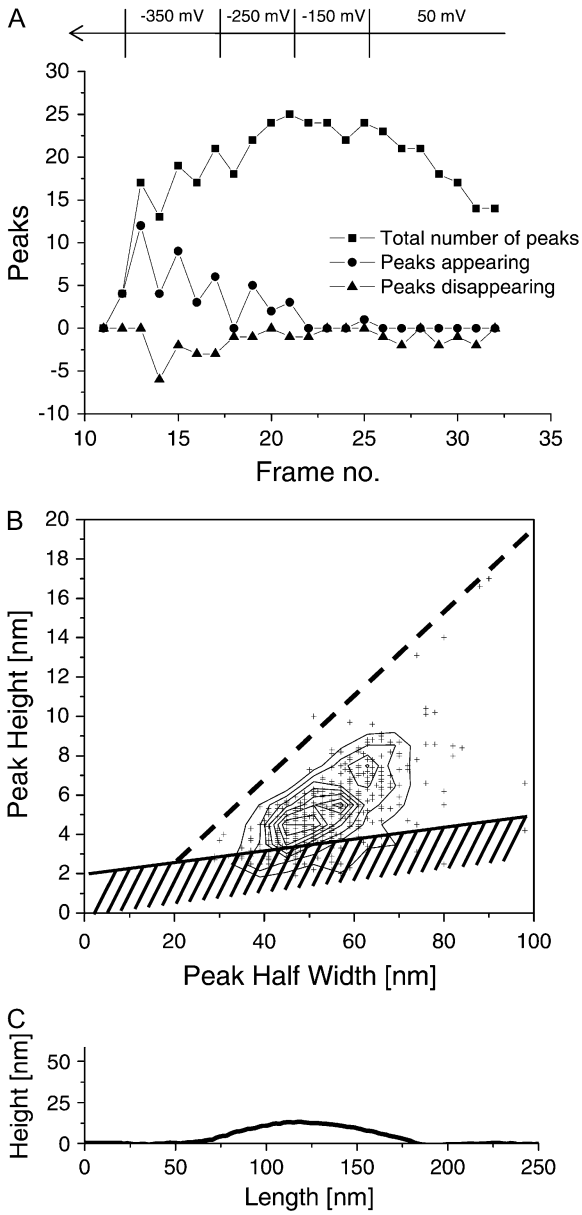

FIGURE 6 (*A*) The number of heightened areas that were visible in a set of AFM images (1 × 1 μm) recorded from the same area while changing the applied potential between scans (as indicated above the graph). Besides the total number of heightened areas, also the number of peaks that appear (and disappear) between consecutive scan is given. Peak areas which appear or disappear due to drift (from the AFM equipment) inside or outside the 1 × 1 μm area were disregarded. (*B*) A two-dimensional correlation plot between the height and half-height-width of the heightened areas. Four-hundred-and-three areas were analyzed. Shaded area in the plot indicates a region where peaks might not have been detected due to noise or nonideal baselines in the AFM images. The dashed line indicates the observed maximum sharpness that the heightened areas can obtain (see text for more information). (*C*) A height-length normalized profile of a heightened area with maximum sharpness, as defined in panel *B*.

surface modified by 6MH (see Fig. 1). One possibility is that when electric fields are applied, pockets of water are formed that push the membrane upwards. The formation of water pockets could be either due to transport of electrolyte through

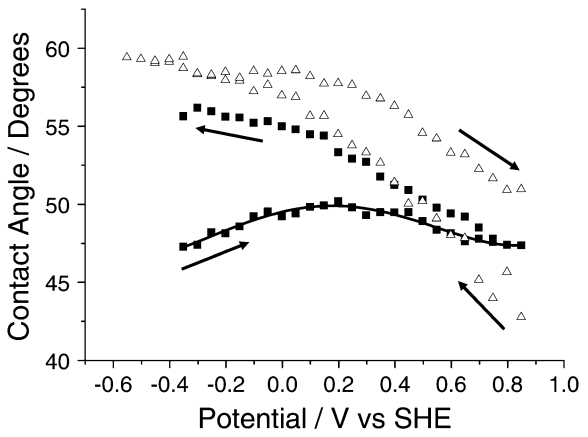

FIGURE 7 Advancing contact angles of a gold surface modified with 6MH as a function of applied potential. Data points are averages of nine (*solid squares*) and five (*open triangles*) experiments. The closed and open data points are measured in the order indicated by the arrows.

the membrane or due to the formation of water. The latter is conceivable, since the AFM experiments were done in air and at negative potentials, some oxygen is reduced to water at the electrode surface. As no pores have been visualized by AFM, the transport of electrolyte through the membrane seems less likely, although the timescale of the AFM imaging (seconds) will not detect short-lived pores. Furthermore, the EIS results indicate an increase in charge transport through the membrane at negative potentials. An alternative explanation for the heightened areas could involve an increase of the membrane area due to the electric field (12,33). An increase of a membrane tethered to a surface would result in areas in which the membrane is forced away from the surface.

Interestingly, a recent article showed that micron-sized areas of SLMs on glass also elevate when phosphatidic-acid containing lipid layers were subjected to asymmetry in ionic strength (34). These heightened areas were not formed by pushing the membrane upwards or an increase in membrane area, but by bending forces within the membrane. The use of SLM systems to study bending mechanisms and membrane curvature has recently been reviewed by Groves (35). To our knowledge, this report shows, for the first time, the curvature of the membrane on the nanometer scale.

I am grateful to Sophie Weiss and Adeela Naz for their help with the contact angle measurements, Mohammed Nurnabi for the synthesis of EO3-cholesterol, and Simon Connell for discussions about the AFM data.

This work was supported by a David Phillips fellowship from the Biotechnology and Biological Sciences Research Council and a Royal Society Research grant.

REFERENCES

1. Tsong, T. 1991. Electroporation of cell membranes. *Biophys. J.* 60: 297–306.
2. Weaver, J. C. 2003. Electroporation of biological membranes from multicellular to nano scales. *IEEE Trans. Dielectrics Electr. Insul.* 10:754–768.

3. Neumann, E., S. Kakorin, and K. Toensing. 1999. Fundamentals of electroporative delivery of drugs and genes. *Bioelectrochem. Bioenerg.* 48:3–16.
4. Krassowska, W., and P. D. Filev. 2007. Modeling electroporation in a single cell. *Biophys. J.* 92:404–417.
5. Tarek, M. 2005. Membrane electroporation: a molecular dynamics simulation. *Biophys. J.* 88:4045–4053.
6. Tieleman, D. P., H. Leontiadou, A. E. Mark, and S. J. Marrink. 2003. Simulation of pore formation in lipid bilayers by mechanical stress and electric fields. *J. Am. Chem. Soc.* 125:6382–6383.
7. Gurtovenko, A. A., and I. Vattulainen. 2005. Pore formation coupled to ion transport through lipid membranes as induced by transmembrane ionic charge imbalance: atomistic molecular dynamics study. *J. Am. Chem. Soc.* 127:17570–17571.
8. Dzubiella, J., and J.-P. Hanson. 2005. Electric-field-controlled water and ion permeation of a hydrophobic nanopore. *J. Chem. Phys.* 122:234706.
9. Vernier, P. T., M. J. Ziegler, Y. Sun, W. V. Chang, M. A. Gundersen, and D. Tieleman. 2006. Nanopore formation and phosphatidylserine externalization in phospholipid bilayer at high transmembrane potential. *J. Am. Chem. Soc.* 128:6288–6289.
10. Pliquett, U., R. P. Joshi, V. Sridhara, and K. H. Schoenbach. 2007. High electrical field effects on cell membranes. *Bioelectrochemistry.* 70:275–282.
11. Rodriguez, N., S. Cribier, and F. Pincet. 2006. Transition from long- to short-lived transient pores in giant vesicles in an aqueous medium. *Phys. Rev. E Stat. Nonlin. Soft Matter Phys.* 74:061902.
12. Riske, K. A., and R. Dimova. 2005. Electro-deformation and poration of giant vesicles viewed with high temporal resolution. *Biophys. J.* 88: 1143–1155.
13. Müller, D. J., K. T. Sapra, S. Scheuring, A. Kedrov, P. L. Frederix, D. Fotiadis, and A. Engel. 2006. Single-molecule studies of membrane proteins. *Curr. Opin. Struct. Biol.* 16:489–495.
14. Quist, A. P., A. Chand, S. Ramachandran, C. Daraio, S. Jin, and R. Lal. 2007. Atomic force microscopy imaging and electrical recording of lipid bilayers supported over microfabricated silicon chip nanopores: lab-on-a-chip system for lipid membranes and ion channels. *Langmuir.* 23:1375–1380.
15. Schabert, F. A., C. Henn, and A. Engel. 1995. Native *Escherichia coli* OmpF porin surfaces probed by atomic-force microscopy. *Science.* 268:92–94.
16. Czajkowsky, D. M., E. M. Hotze, Z. F. Shao, and R. K. Tweten. 2004. Vertical collapse of a cytolysin prepore moves its transmembrane β-hairpins to the membrane. *EMBO J.* 23:3206–3215.
17. Fotiadis, D., B. Jastrzebska, A. Philippsen, D. J. Muller, K. Palczewski, and A. Engel. 2006. Structure of the rhodopsin dimer: a working model for G-protein-coupled receptors. *Curr. Opin. Struct. Biol.* 16:252–259.
18. Mou, J. X., J. Yang, C. Huang, and Z. F. Shao. 1994. Alcohol induces interdigitated domains in unilamellar phosphatidylcholine bilayers. *Biochemistry.* 33:9981–9985.
19. Mou, J. X., J. Yang, and Z. F. Shao. 1994. Tris(hydroxymethyl)aminomethane ($C_4H_{11}NO_3$) induced a ripple phase in supported unilamellar phospholipid bilayers. *Biochemistry.* 33:4439–4443.
20. Dufrêne, Y. F., and G. U. Lee. 2000. Advances in the characterization of supported lipid films with the atomic force microscope. *Biochim. Biophys. Acta Biomembr.* 1509:14–41.
21. Connell, S. D., and D. A. Smith. 2006. The atomic force microscope as a tool for studying phase separation in lipid membranes. *Mol. Membr. Biol.* 23:17–28 [Review].
22. Richter, R. P., R. Berat, and A. R. Brisson. 2006. Formation of solid-supported lipid bilayers: an integrated view. *Langmuir.* 22:3497–3505.
23. Boden, N., R. J. Bushby, S. Clarkson, S. D. Evans, P. F. Knowles, and A. Marsh. 1997. The design and synthesis of simple molecular tethers for binding biomembranes to a gold surface. *Tetrahedron.* 53:10939–10952.
24. Stamou, D., D. Gourdon, M. Liley, N. A. Burnham, A. Kulik, H. Vogel, and C. Duschl. 1997. Uniformly flat gold surfaces: imaging the domain structure of organic monolayers using scanning force microscopy. *Langmuir.* 13:2425–2428.
25. Jeuken, L., N. N. Daskalakis, X. Han, K. Sheikh, A. Erbe, R. Bushby, and S. Evans. 2007. Phase separation in mixed self-assembled monolayers and its effect on biomimetic membranes. *Sens. Actuators B.* 124:501–509.
26. Jeuken, L. J. C., S. D. Connell, P. J. F. Henderson, R. B. Gennis, S. D. Evans, and R. J. Bushby. 2006. Redox enzymes in tethered membranes. *J. Am. Chem. Soc.* 128:1711–1716.
27. Abbott, N. L., D. R. Rolison, and G. M. Whitesides. 1994. Combining micromachining and molecular self-assembly to fabricate microelectrodes. *Langmuir.* 10:2672–2682.
28. Iwami, Y., D. Hobara, M. Yamamoto, and T. Kakiuchi. 2004. Determination of the potential of zero charge of Au^{111} electrodes modified with thiol self-assembled monolayers using a potential-controlled sessile drop method. *J. Electroanal. Chem.* 564:77–83.
29. Sondag-Huethorst, J. A. M., and L. G. J. Fokkink. 1995. Electrochemical characterization of functionalized alkanethiol monolayers on gold. *Langmuir.* 11:2237–2241.
30. Boubour, E., and R. B. Lennox. 2000. Stability of ω-functionalized self-assembled monolayers as a function of applied potential. *Langmuir.* 16:7464–7470.
31. Valincius, G., D. J. McGillivray, W. Febo-Ayala, D. J. Vanderah, J. J. Kasianowicz, and M. Lösche. 2006. Enzyme activity to augment the characterization of tethered bilayer membranes. *J. Phys. Chem. B.* 110: 10213–10216.
32. McGillivray, D. J., G. Valincius, D. J. Vanderah, W. Febo-Ayala, J. T. Woodward, F. Heinrich, J. Kasianowicz, and M. Lösche. 2007. Molecular-scale structural and functional characterization of sparsely tethered bilayer lipid membranes. *Biointerphases.* 2:21–31.
33. Needham, D., and R. M. Hochmuth. 1989. Electro-mechanical permeabilization of lipid vesicles. *Biophys. J.* 55:1001–1009.
34. Cambrea, L. R., and J. S. Hovis. 2007. Formation of three-dimensional structures in supported lipid bilayers. *Biophys. J.* 92:3587–3594.
35. Groves, J. T. 2007. Bending mechanics and molecular organization in biological membranes. *Annu. Rev. Phys. Chem.* 58:697–717.